Estimation of geometric properties of three-component sinusoidal signals for system monitoring

Gailene Phua and Pierre Granjon

GIPSA-lab - Grenoble Campus
11 rue des Mathématiques, BP 46, 38402 Saint-Martin-d'Hères, France
{gailene.phua, pierre.granjon}@gipsa-lab.grenoble-inp.fr

Abstract

The estimation of the geometric properties of the elliptical trajectory followed by a three-component sinusoidal signal in three-dimensional Euclidean space with the objective of system monitoring is addressed in this paper. In system monitoring problems, multicomponent signals are frequently encountered. Most physical quantities are naturally composed of three components. In this paper, a three-component sinusoidal signal is studied. Three sinusoids of the same frequency follow a trajectory in the shape of an ellipse when plotted in three-dimensional Euclidean space. It is the geometric properties of this elliptical trajectory that are estimated in this paper. The geometric properties of interest are the norm of the position vector, the binormal vector, curvature and torsion. Straightforward expressions of these quantities are given which allow the geometric properties of the ellipse to be recovered from three-component data. Definition and interpretation of the expressions are also included, followed by a step-by-step explanation of the approach used to estimate these quantities. The performance and limitations of the method with respect to various parameters such as noise, frequency of the sinusoids and ellipticity are discussed. The usefulness of this method as an informative means of describing three-component sinusoidal signals is illustrated with two applications.

1 Introduction

Multicomponent signals are frequently encountered in system monitoring applications. Most physical quantities are naturally composed of three components. Examples include three-dimensional displacements for mechanical systems and, more artificially, three-phase electrical quantities for electrical systems. In order to obtain efficient fault indicators, such three-component signals can be analyzed with the usual marginal and/or joint analysis tools in the time domain (by using correlation functions and/or correlation matrices) as well as in the frequency domain (spectra and/or spectral matrices) [1]. However, three-component signals also contain another type of information which is completely different in nature: their geometric properties. The geometric nature and properties of the trajectory followed by such data in three-dimensional Euclidean space can be related to the state of the system from which the data have been acquired. This approach has already been successfully proposed in the field of system monitoring with two-component signals [2] by using complex-valued signal processing tools [3]. It is the case for orbit shape analysis used to detect faults in rotating machines [4, 5, 6], and for voltage dips detection and classification in power networks [7]. In this paper, this approach is generalized to three-component signals by using basic differential geometry concepts such as the Frenet-Serret frame and related geometric quantities.

The foundations of the proposed method are presented first. These include the definition of the three-component signal of interest as well as the geometric properties to be estimated. This is followed by the explanation of the algorithm used to estimate the geometric properties. Next, the details of the estimation performance of the algorithm with respect to various parameters are presented. To illustrate the usefulness of the method, two application examples are shown. Finally, the paper ends with a conclusion including a summary and suggestions of possible future work.

2 Method foundations

In this section, the definition of the three-component sinusoidal signals that are studied in this paper is given, followed by the presentation of its trajectory in three-dimensional Euclidean space and the definition of its geometric properties. These definitions are the foundations of the proposed method and are used throughout the paper.

2.1 Definiton of three-component sinusoidal signals

In this paper, a signal is considered to be a three-component sinusoidal signal if it can be represented as a matrix of three rows of data where each row corresponds to one component of the signal and where the three components are each a sine wave of the same fundamental frequency f_0. A three-component sinusoidal signal $\mathbf{r}$ can therefore be written mathematically as in Eq. (1) where, for $i \in \{1,\ 2,\ 3\}$, A_i and φ_i denote the amplitude and phase of the sinusoids respectively.

$$\mathbf{r}(t) = \begin{bmatrix} r_1(t) \\ r_2(t) \\ r_3(t) \end{bmatrix} = \begin{bmatrix} A_1 \sin(2\pi f_0 t + \varphi_1) \\ A_2 \sin(2\pi f_0 t + \varphi_2) \\ A_3 \sin(2\pi f_0 t + \varphi_3) \end{bmatrix} \tag{1}$$

Equation (1) shows that $\mathbf{r}$ is a parametrized differentiable curve and the variable t is called the parameter of the curve [8]. In other words, $\mathbf{r}$ is a differentiable map $\mathbf{r}\colon \mathbb{R} \to \mathbb{R}^3$ of the real line $\mathbb{R}$ into $\mathbb{R}^3$, the set of triples of real numbers. This means that $\mathbf{r}$ maps each $t \in \mathbb{R}$ into a point $\mathbf{r}(t) = [r_1(t),\ r_2(t),\ r_3(t)] \in \mathbb{R}^3$ and the functions r_1, r_2 and r_3 are differentiable. For example, if $r_1'(t)$ denotes the first derivative of r_1 at the point t and similar notations are used for the functions r_2 and r_3, the notation for the first derivative of $\mathbf{r}$ is $\mathbf{r}'(t) = [r_1'(t),\ r_2'(t),\ r_3'(t)] \in \mathbb{R}^3$.

2.2 Trajectory in three-dimensional Euclidean space

There are many ways to plot a three-component sinusoidal signal. Figure 1 shows two ways of plotting the three-component sinusoidal signal $\mathbf{r}$ with fundamental frequency $f_0 = 10$ Hz, amplitude $A_1 = A_2 = A_3 = 1$ and phase $[\varphi_1,\ \varphi_2,\ \varphi_3] = \left[0,\ \frac{3\pi}{7},\ \frac{8\pi}{7}\right]$. In Fig. 1(a), each of the three components of $\mathbf{r}$ is plotted separately with respect to the parameter t. In Fig. 1(b), the same signal $\mathbf{r}$ is represented in three-dimensional Euclidean space where each component follows one axis of the space. The second plot shows a space curve which is the image set $\mathbf{r}(\mathbb{R}) \subset \mathbb{R}^3$ called the trace of $\mathbf{r}$ [8]. The plot in Fig. 1(b) is the representation of interest in this paper. It can be shown that a three-component sinusoidal signal follows an elliptical trajectory when plotted in three-dimensional Euclidean space, as can be seen in Fig. 1(b). This trajectory is characterized by several geometric properties related to its shape and osculating plane. It is these geometric properties that we are looking to estimate in this paper, with the objective of using them to characterize the condition of the system from which the three-component sinusoidal signal is acquired. These geometric properties are defined in the next section by using basic differential geometry tools such as the Frenet frame. In what follows, the trace of $\mathbf{r}$ is also called trajectory or space curve.

(a) Plot of $\mathbf{r}$ with respect to t

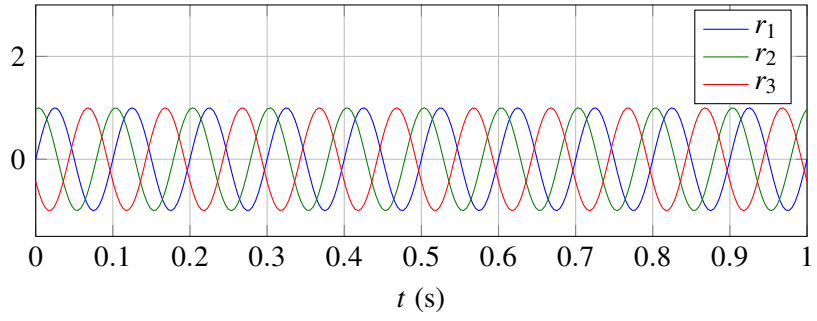

(b) Plot of $\mathbf{r}$ in 3D Euclidean space

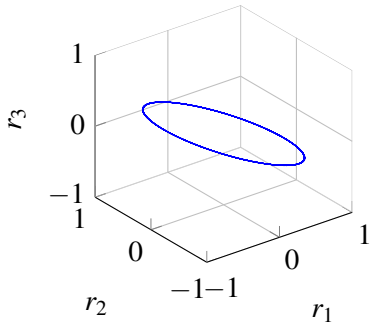

Figure 1: Two different representations of the same three-component sinusoidal signal, $\mathbf{r}$

2.3 Geometric properties and Frenet frame

The three-component sinusoidal signal is called $\mathbf{r}$ for the radius vector, also known as the position vector, because the vector $\mathbf{r}(t)$ defines a position from the origin at any time t on the elliptical trajectory. The norm, or the length, of the vector $\mathbf{r}(t)$, denoted by $\|\mathbf{r}(t)\|$, is a first and simple interesting geometric property since it gives an idea of the size of the ellipse followed by $\mathbf{r}(t)$. An approximation of the length of the semimajor axis a and semiminor axis b of the ellipse can be deduced from the time evolution of $\|\mathbf{r}(t)\|$ (see Fig. 2). In the case of noiseless signals, as in the example of Fig. 1, the shape of the trajectory is a perfect ellipse and the maximum and minimum values of $\|\mathbf{r}(t)\|$ (Fig. 2(b)) are equal to the length of the semimajor and semiminor axes respectively (Fig. 2(c)).

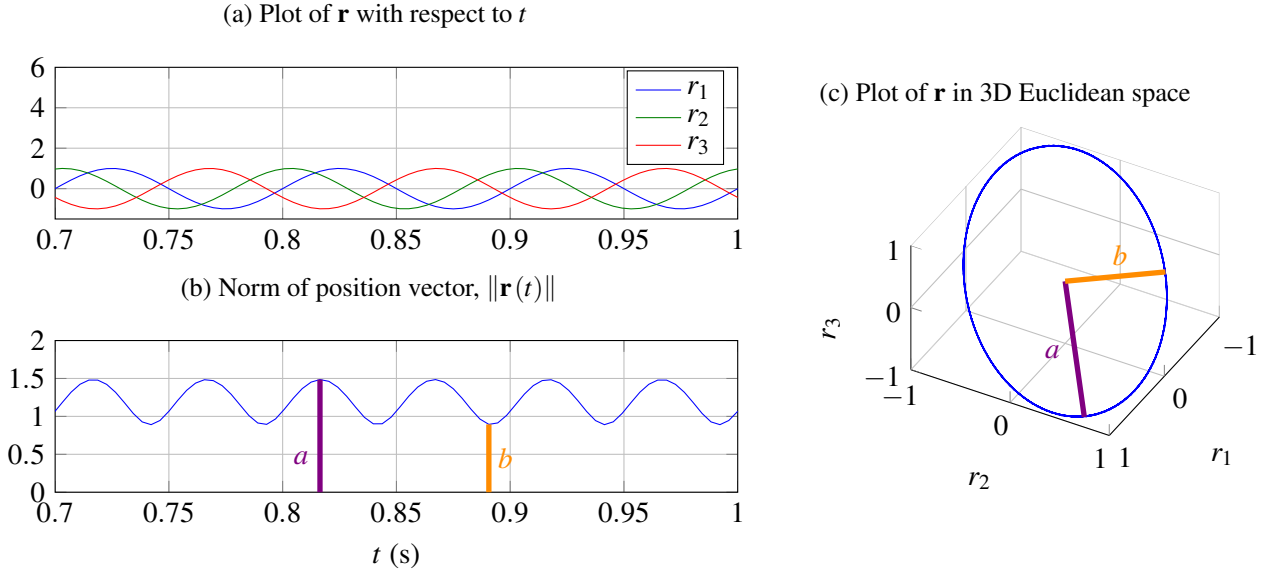

Figure 2: Estimation of the semimajor axis a and semiminor axis b of the ellipse in Fig. 1

Equation (2) is used to calculate this first geometric property.

$$\|\mathbf{r}(t)\| = \sqrt{r_1(t)^2 + r_2(t)^2 + r_3(t)^2} \tag{2}$$

Space curves can also be locally characterized by other geometric properties such as curvature, torsion and the Frenet frame. Instead of a global reference frame like the Euclidean coordinates, a local reference frame called the Frenet frame (or the Frenet-Serret frame) can be used to describe the space curve locally at each point $\mathbf{r}(t)$ as well as to compute its local geometric properties including curvature and torsion [9]. The Frenet frame is a moving reference frame defined by three orthonormal vectors, the tangent, normal and binormal vectors, at each point of the curve. For each point $\mathbf{r}(t)$ of a smooth (continuous and differentiable) space curve, the tangent $\mathbf{T}$, normal $\mathbf{N}$ and binormal $\mathbf{B}$ vectors are given by Eq. (3), (4) and (5) [9, 10] where $\mathbf{r}'(t)$ denotes $\frac{\mathrm{d}\mathbf{r}(t)}{\mathrm{d}t}$ and $\times$ denotes the cross product.

$$\mathbf{T}(t) = \frac{\mathbf{r}'(t)}{\|\mathbf{r}'(t)\|} \tag{3}$$

$$\mathbf{N}(t) = \frac{\mathbf{T}'(t)}{\|\mathbf{T}'(t)\|} = \frac{\mathbf{r}'(t) \times (\mathbf{r}''(t) \times \mathbf{r}'(t))}{\|\mathbf{r}'(t)\| \, \|\mathbf{r}''(t) \times \mathbf{r}'(t)\|} \tag{4}$$

$$\mathbf{B}(t) = \mathbf{T}(t) \times \mathbf{N}(t) = \frac{\mathbf{r}'(t) \times \mathbf{r}''(t)}{\|\mathbf{r}'(t) \times \mathbf{r}''(t)\|} \tag{5}$$

The three unit vectors of the Frenet frame are illustrated in Fig. 3. The tangent vector $\mathbf{T}(t)$ at a particular point $\mathbf{r}(t)$ of the trajectory shows the direction the point is moving in. The normal vector $\mathbf{N}(t)$ represents the direction of change in the tangent vector. The plane described by the tangent and normal vectors is called the osculating plane (Fig. 3(b)), which is also the plane the trajectory is in around $\mathbf{r}(t)$. Equation (5) shows that the binormal vector $\mathbf{B}(t)$ is orthogonal to $\mathbf{T}(t)$ and $\mathbf{N}(t)$, and therefore to the osculating plane. This means that

$\mathbf{B}(t)$ alone can be used to define this plane completely. Equation (5) sums up the relationship between the three Frenet vectors and shows that they are orthogonal to each other following the right-hand rule.

(a) The Frenet frame at point $\mathbf{r}(t)$ (b) Osculating plane

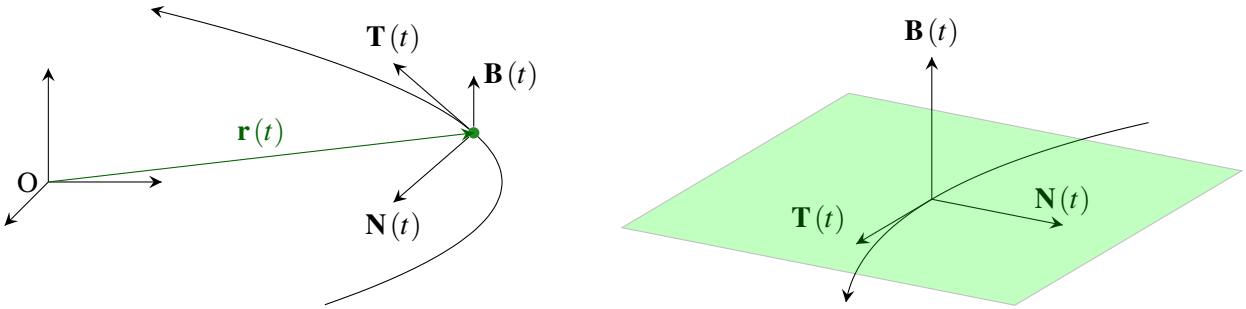

Figure 3: The tangent $\mathbf{T}(t)$, normal $\mathbf{N}(t)$ and binormal $\mathbf{B}(t)$ vectors of the Frenet frame at a point $\mathbf{r}(t)$

The Frenet frame obeys the three differential equations (also known as the Frenet-Serret formulas) written in matrix form in Eq. (6), where the scalars $\kappa(t)$ and $\tau(t)$ are respectively the curvature and the torsion of the curve at point $\mathbf{r}(t)$.

$$\begin{bmatrix} \mathbf{T}'(t) \\ \mathbf{N}'(t) \\ \mathbf{B}'(t) \end{bmatrix} = \|\mathbf{r}'(t)\| \begin{bmatrix} 0 & \kappa(t) & 0 \\ -\kappa(t) & 0 & \tau(t) \\ 0 & -\tau(t) & 0 \end{bmatrix} \begin{bmatrix} \mathbf{T}(t) \\ \mathbf{N}(t) \\ \mathbf{B}(t) \end{bmatrix} \tag{6}$$

From the first line of Eq. (6), we see that $\|\mathbf{T}'(t)\| = \|\mathbf{r}'(t)\| \, |\kappa(t)|$. The curvature is therefore related to the rate of change of the tangent vector $\mathbf{T}(t)$, and represents the tendency of $\mathbf{r}(t)$ to deviate from the local direction of the movement. Thus, $\kappa(t)$ tells us how sharp the trajectory is curving at any one point. The sharper the bend, the greater the curvature. For example, the curvature of a circle is constant at each point of the circle and is equal to the reciprocal of its radius (a small circle has greater curvature than a big circle).

Similarly, the third line of Eq. (6) leads to $\|\mathbf{B}'(t)\| = \|\mathbf{r}'(t)\| \, |\tau(t)|$. Hence, the torsion $\tau(t)$ is directly related to the rate of change of the binormal vector $\mathbf{B}(t)$ and shows the tendency of $\mathbf{r}(t)$ to deviate from the osculating plane. For example, the torsion is zero if the trajectory stays in the same plane but increases when the trajectory changes planes.

The curvature and torsion can be expressed as a function of $\mathbf{r}(t)$ as in Eq. (7) and (8) [11, 12], where $\cdot$ denotes the dot product.

$$\kappa(t) = \frac{\|\mathbf{r}'(t) \times \mathbf{r}''(t)\|}{\|\mathbf{r}'(t)\|^3} \tag{7}$$

$$\tau(t) = \frac{\big(\mathbf{r}'(t) \times \mathbf{r}''(t)\big) \cdot \mathbf{r}'''(t)}{\|\mathbf{r}'(t) \times \mathbf{r}''(t)\|^2} \tag{8}$$

The geometric quantities presented above can be used to locally characterize the geometry of the trajectory followed by a three-component sinusoidal signal and one possible algorithm to estimate these quantities is explained in the following section.

3 Estimation algorithm

With the objective of characterizing the geometry of the trajectory followed by the three-component sinusoidal signal, we have chosen to estimate four geometric properties:

- the magnitude of the position vector, $\|\mathbf{r}(t)\|$
- the binormal vector, $\mathbf{B}(t)$
- curvature, $\kappa(t)$
- torsion, $\tau(t)$

In this section, the algorithm used to estimate these geometric properties is presented. It is based on Eq. (2), (5), (7) and (8) which show that these quantities can be calculated in terms of the values $\mathbf{r}(t)$ of the position

vector and its first three derivatives. Figure 4 is a block diagram representing the three main steps of this algorithm.

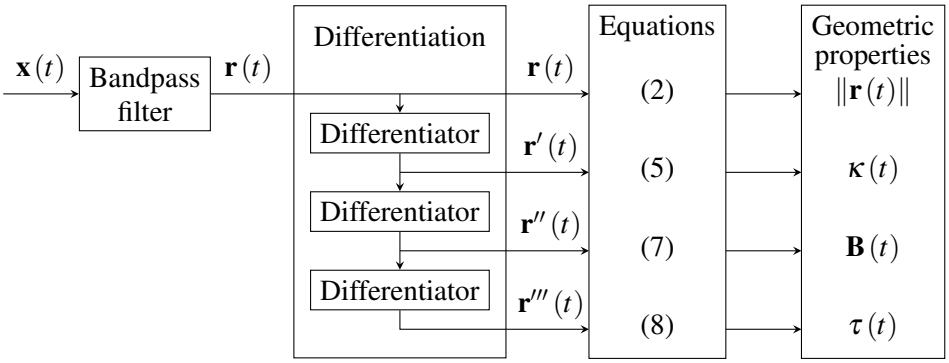

Figure 4: Block diagram of the estimation algorithm

The first step involves filtering the measured three-component signal $\mathbf{x}$. Measured signals usually contain more than one frequency component including noise. It is therefore essential to filter such signals first to remove noise and all unwanted frequency components leaving only one frequency component f_0. To carry out this step, a linear phase FIR filter [13, 14] which can be a lowpass, bandpass or highpass filter is used. The suitable filter is chosen according to the frequency f_0 of the signal we want to study. This step produces the three-component sinusoidal signal $\mathbf{r}$ following an elliptical trajectory from which we will be able to compute the geometric properties.

From the definition of the geometric properties, the next necessary step is the differentiation of $\mathbf{r}$. For this step, a linear phase FIR differentiator filter is used. Instead of a full band differentiator, a partial band differentiator is used in order to avoid amplifying possible residual high frequency components and maximize the output signal-to-noise ratio (SNR) [15]. As with the first step, this differentiator filter has a bandwidth adapted to f_0 as shown in Fig. 5. Since $\mathbf{r}$ needs to be differentiated three times, the differentiator filter is applied three times consecutively to $\mathbf{r}$.

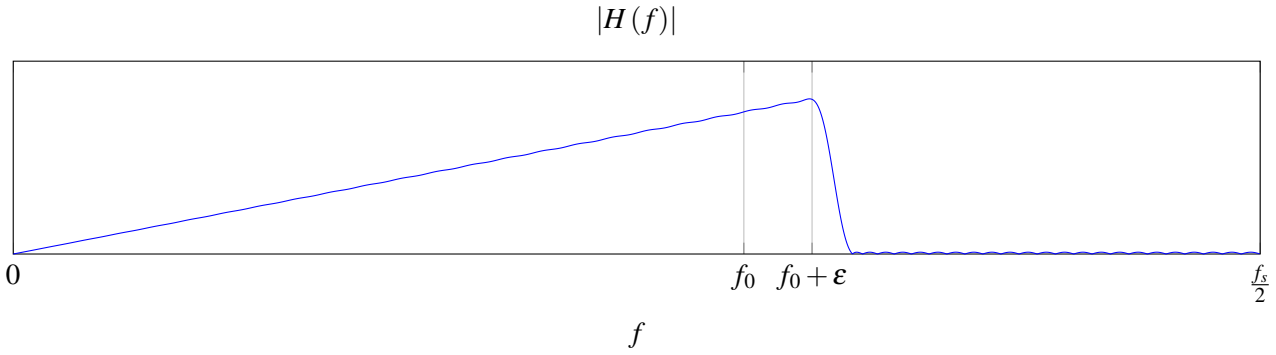

Figure 5: Frequency response magnitude of the partial band differentiator

The final step of Fig. 4 is to compute the desired geometric properties using Eq. (2), (5), (7) and (8), where only basic mathematical operators (division, vector norm, dot product, cross product) are needed.

The proposed algorithm only uses FIR filters and simple instantaneous operators, hence can be easily implemented in real time. Its estimation performance is detailed in the next section.

4 Estimation performance of algorithm

Testing a method on simulated signals first before applying it to real signals is essential to know how well it works in different conditions. In this section, the performance of the algorithm as well as its limits with respect to various parameters are discussed. Three parameters which influence the accuracy of the method have been

identified: the amount of noise present in the signal, the frequency of the three-component signal f_0 and the ellipticity (flatness) of the ellipse.

The performance of the method is measured using the mean squared error (MSE) of the estimators $\|\hat{\mathbf{r}}\|$, $\hat{\mathbf{B}}$, $\hat{\kappa}$ and $\hat{\tau}$. The equations used to compute the four MSE are given by Eq. (9), (10), (11) and (12) for discrete-time signals where N represents the number of samples of the signals.

- MSE of the magnitude of the position vector $\text{MSE}_{\|\mathbf{r}\|}$ where $\|\mathbf{r}\|$ and $\|\hat{\mathbf{r}}\|$ are the theoretical and estimated values of the magnitude of the position vector respectively:

$$\text{MSE}_{\|\mathbf{r}\|} = \frac{\sum_{k=1}^{N} \left(\|\mathbf{r}[k]\| - \|\hat{\mathbf{r}}[k]\|\right)^2}{\sum_{k=1}^{N} \|\mathbf{r}[k]\|^2} \tag{9}$$

- MSE of the binormal vector $\text{MSE}_{\mathbf{B}}$ where $\mathbf{B}$ and $\hat{\mathbf{B}}$ are the theoretical and estimated values of the binormal vector respectively:

$$\text{MSE}_{\mathbf{B}} = \frac{\sum_{i=1}^{3} \left(\frac{1}{N} \sum_{k=1}^{N} \left(\mathbf{B}_i - \hat{\mathbf{B}}_i[k]\right)^2 \right)}{\sum_{i=1}^{3} \mathbf{B}_i^2} = \sum_{i=1}^{3} \left(\frac{1}{N} \sum_{k=1}^{N} \left(\mathbf{B}_i - \hat{\mathbf{B}}_i[k]\right)^2 \right) \tag{10}$$

  where $\mathbf{B}_i$ is the ith component of $\mathbf{B}$ which is a unit vector $\left(\sum_{i=1}^{3} \mathbf{B}_i^2 = 1 \right)$.

- MSE of the curvature MSE_{κ} where κ and $\hat{\kappa}$ are the theoretical and estimated values of the curvature respectively:

$$\text{MSE}_{\kappa} = \frac{\sum_{k=1}^{N} \left(\kappa[k] - \hat{\kappa}[k]\right)^2}{\sum_{k=1}^{N} \kappa[k]^2} \tag{11}$$

- MSE of the torsion MSE_{τ} where $\hat{\tau}$ represents the estimated values of the torsion:

$$\text{MSE}_{\tau} = \frac{1}{N} \sum_{k=1}^{N} \hat{\tau}[k]^2 \tag{12}$$

  This MSE is not normalized contrary to the previous ones, because the theoretical value of τ is zero for a three-component sinusoidal signal with only one frequency component and constant amplitude and phase.

The influence of the SNR, the signal frequency and the ellipticity on how well the method works is presented next. For each parameter, the type of simulated three-component sinusoidal signal used is mentioned at the beginning, followed by graphs illustrating the results of the tests. The MSE plotted in the graphs is the average of 100 MSE obtained through Monte Carlo simulations.

4.1 Performance with respect to SNR

A 40-second discrete-time three-component sinusoidal signal $\mathbf{x}$ given by Eq. (13) with fundamental frequency $f_0 = 10$ Hz and sampling frequency $f_s = 256$ Hz is generated.

$$\mathbf{x}[k] = \begin{bmatrix} x_1[k] \\ x_2[k] \\ x_3[k] \end{bmatrix} = \begin{bmatrix} A_1 \sin(2\pi f_0 k T_s + \varphi_1) \\ A_2 \sin(2\pi f_0 k T_s + \varphi_2) \\ A_3 \sin(2\pi f_0 k T_s + \varphi_3) \end{bmatrix} \tag{13}$$

All sinusoids have the same amplitude, $A_1 = A_2 = A_3 = 20$, and their initial phase are $\varphi_1 = 0$, $\varphi_2 = \frac{3\pi}{7}$ and $\varphi_3 = \frac{8\pi}{7}$ rad. Such a signal follows a trajectory in the shape of an ellipse with semimajor axis $a = 29.71$ and semiminor axis $b = 17.81$. The ellipticity, denoted here as $\frac{b}{a}$, is therefore 0.5994. The binormal vector $\mathbf{B}$ is constant in this case with the values:

$$\mathbf{B}[k] = \begin{bmatrix} \mathbf{B}_1 \\ \mathbf{B}_2 \\ \mathbf{B}_3 \end{bmatrix} = \begin{bmatrix} 0.5910 \\ 0.7370 \\ -0.3280 \end{bmatrix} \tag{14}$$

An additive white Gaussian noise with a variance σ_i^2 is added to each component x_i. The amount of noise is given by the $\mathrm{SNR}_{\mathrm{dB}}$ defined as $10\log_{10}\frac{A_i^2}{2\sigma_i^2}$. For the sake of simplicity, the same SNR is used for all components.

Figures 6(a)-(d) show the relationship between this $\mathrm{SNR}_{\mathrm{dB}}$ and the MSE of the four estimators. From the graphs, it can be deduced that the greater the SNR, the smaller the error, as expected. The worst estimation error is obtained for the curvature κ. This can be due to the fact that $\hat{\kappa}$ is the only estimator that uses derivatives of $\mathbf{r}(t)$ and estimates a time-varying quantity. $\|\hat{\mathbf{r}}\|$ estimates a time-varying quantity without differentiators, while $\hat{\mathbf{B}}$ and $\hat{\tau}$ need differentiators but estimate constant values.

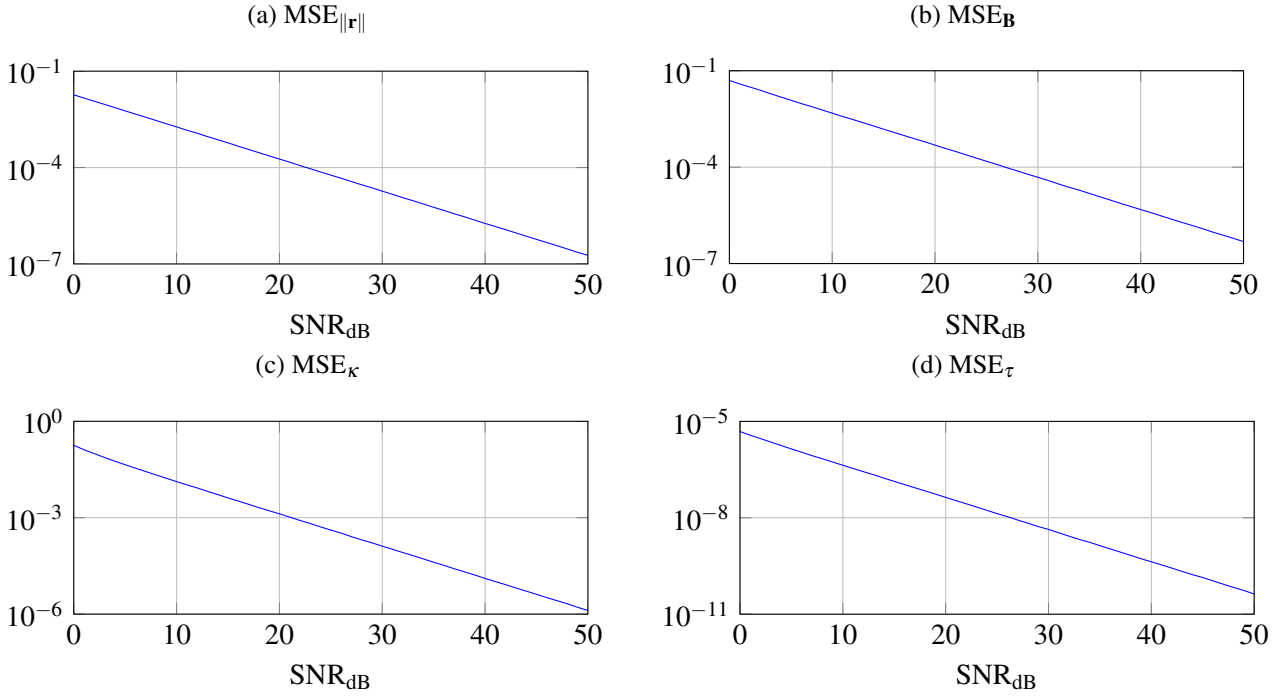

Figure 6: MSE of four estimators with respect to SNR

4.2 Performance with respect to signal frequency

The three-component sinusoidal signal $\mathbf{x}$ is the same as in the previous case. The only difference is that the amount of noise added to the signal is fixed at $\mathrm{SNR}_{\mathrm{dB}} = 20$ dB and that the fundamental frequency f_0, which is now the parameter of interest, varies between 6 and 122 Hz (with a resolution of 1 Hz).

The corresponding MSE are shown in Figures 7(a)-(d). These figures clearly show that $\mathrm{MSE}_{\|\mathbf{r}\|}$ is independent of f_0 while the other MSE increase when f_0 is very low compared to the sampling frequency. Contrary to $\|\hat{\mathbf{r}}\|$, estimators $\hat{\mathbf{B}}$, $\hat{\kappa}$, $\hat{\tau}$ all use derivatives of $\mathbf{r}(t)$, and one can think that this decrease in performance is due to the FIR differentiator filter. However, a theoretical study, not detailed in this paper, clearly shows that this phenomenon is due to the residual noise left by the first bandpass filter of the proposed algorithm. It is this noise which deteriorates the SNR at the output of each differentiator.

4.3 Performance with respect to ellipticity

In this paper, the ellipticity of the trajectory is measured using the ratio between the semimajor axis a and the semiminor axis b of the ellipse. This quantity $\frac{b}{a}$ can vary between 0 (trajectory=line) and 1 (trajectory=circle).

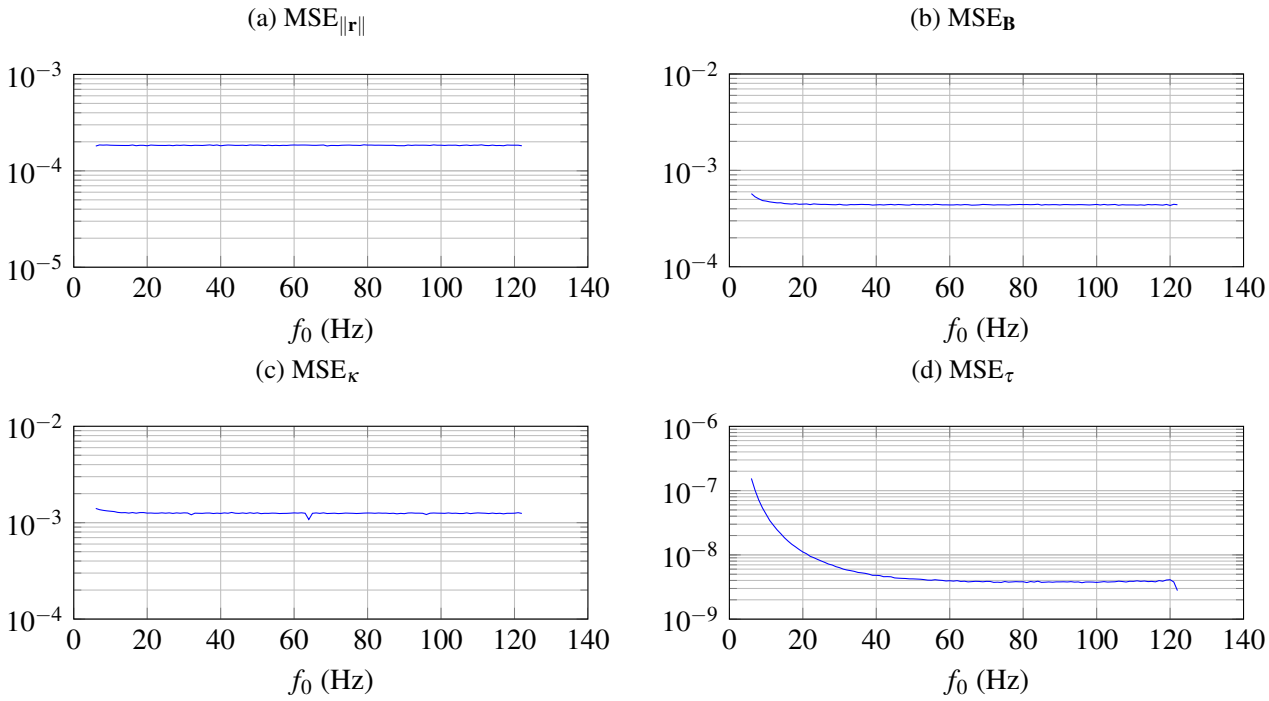

Figure 7: MSE of four estimators with respect to signal frequency

Once again, we use the same three-component sinusoidal signal $\mathbf{x}$, with $\mathrm{SNR}_{\mathrm{dB}} = 20$ dB and $f_0 = 10$ Hz. The parameter of interest is now the ellipticity of the trajectory $\frac{b}{a}$ which varies from 0.1 to 1. To do this, we keep the same amplitude for the sinusoids, $A_1 = A_2 = A_3 = 20$, but change their initial phase φ_1, φ_2 and φ_3. Note that doing this also changes the value of the binormal vector $\mathbf{B}$.

The results are illustrated in Fig. 8(a)-(d). For the magnitude of the position vector $\|\mathbf{r}\|$, the error is constant whatever the flatness of the ellipse. On the contrary, the MSE of the other estimators are not independent of the ellipticity and the nearer the ellipse is to a circle, the smaller the errors. The reason for this is still unclear to us at the moment and we shall investigate this point further.

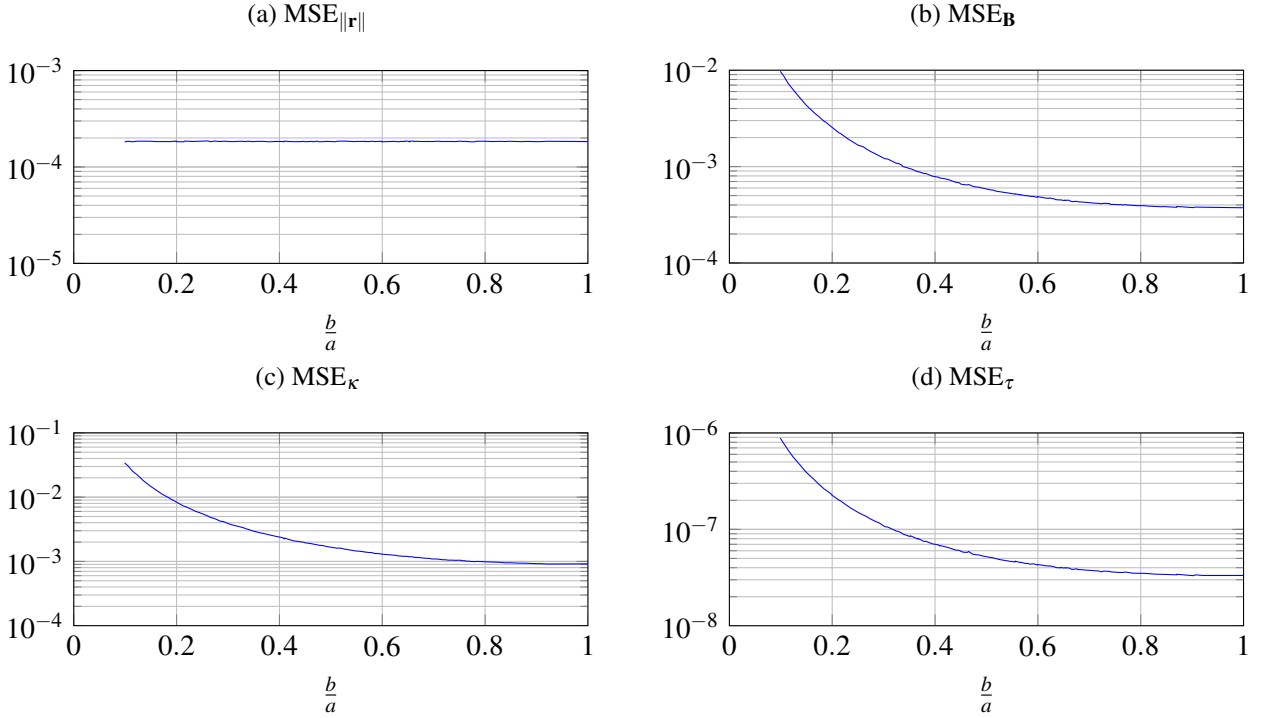

Figure 8: MSE of four estimators with respect to ellipticity

From these performance tests, several things should be kept in mind before applying the method. A lot of noise in the measured signal deteriorates the estimation performance of the algorithm, especially when the signal frequency is low compared to the sampling frequency. Moreover, if the signal follows a trajectory that is almost a line or a very flat ellipse, bear in mind that the algorithm will produce higher estimation errors.

5 Application examples

The proposed method has been applied to three-component sinusoidal signals of low frequency [16] and is now extended to signals of arbitrary frequency. The usefulness of this method as an informative means of describing three-component sinusoidal signals is illustrated with an application to a simulated signal and an experimental signal.

5.1 Simulated signal

The proposed method is first applied to a simulated signal in order to illustrate the tracking capabilities of this algorithm. This three-component signal contains only one frequency component f_0 with a white Gaussian additive noise corresponding to a SNR of 20 dB. A change is introduced in the amplitude and phase of each sinusoid between 4.50 and 4.55 s, leading to a continuous change in the shape of the trajectory and therefore in its geometric properties. The results are shown in Fig. 9.

The measured signal is represented in Fig. 9(c) and the corresponding trajectory in Fig. 9(a), where the influence of noise is clearly visible. The bandpass filtered signal is shown in Fig. 9(b) and the corresponding trajectory in Fig. 9(d), where the noise has been significantly attenuated. The change in the signal characteristics is visible in Fig. 9(d) and the corresponding geometric change in Fig. 9(b). Figures 9(e)-(h) show the estimated geometric properties. As expected, $\|\hat{\mathbf{r}}[k]\|$ and $\hat{\kappa}[k]$ are time-varying because of the elliptic shape of the trajectory. The variations of these two quantities are greater before the change than after. This shows that the elliptical trajectory followed by $\hat{\mathbf{r}}[k]$ is flatter before the change than after. The binormal vector and torsion are more related to the osculating plane. Figures 9(g) and 9(h) show that $\hat{\mathbf{B}}[k]$ and $\hat{\tau}[k]$ are nearly constant when the signal characteristics (amplitude and phase) are constant. This means that the trajectory has a constant osculating plane during these parts of the signal. Nevertheless, $\hat{\mathbf{B}}[k]$ has different coordinates before and after the change corresponding to two different osculating planes. Finally, the torsion $\hat{\tau}[k]$ takes large values only during the change highlighting a change in the osculating plane and could be useful as a change detector.

5.2 Experimental signal

The experimental signal is measured on an induction motor running at a constant rotating frequency of 14.7 Hz. Three accelerometers are placed on this engine to measure its vibrations in three orthogonal directions. The output of the sensors are acquired by an acquisition system containing anti-aliasing filters. The chosen sampling frequency is 256 Hz and the length of the signal is about 10000 samples. The objective here is to characterize the geometric properties of the engine movement at the rotating frequency. Therefore, the proposed algorithm is used to characterize the geometry of the measured vibrations around this rotating frequency. The central frequency of the initial bandpass filter is thus set to 14.7 Hz. The results obtained are shown in Fig. 10. Fig. 10(a) and 10(c) show that the measured signal contains several frequency components and noise. Fig. 10(b) and 10(d) show that the bandpass-filtered signal is composed of only one component of frequency 14.7 Hz, as desired. We see that in Fig. 10(e) and 10(f), $\|\hat{\mathbf{r}}[k]\|$ and $\hat{\kappa}[k]$ are time-varying which means that the trajectory followed by the signal is elliptic at this particular frequency. Next, Fig. 10(g) and 10(h) show that the osculating plane is nearly constant despite small oscillations highlighted by the torsion. This simple example shows that our method facilitates analysis of the geometry of a movement at a given frequency.

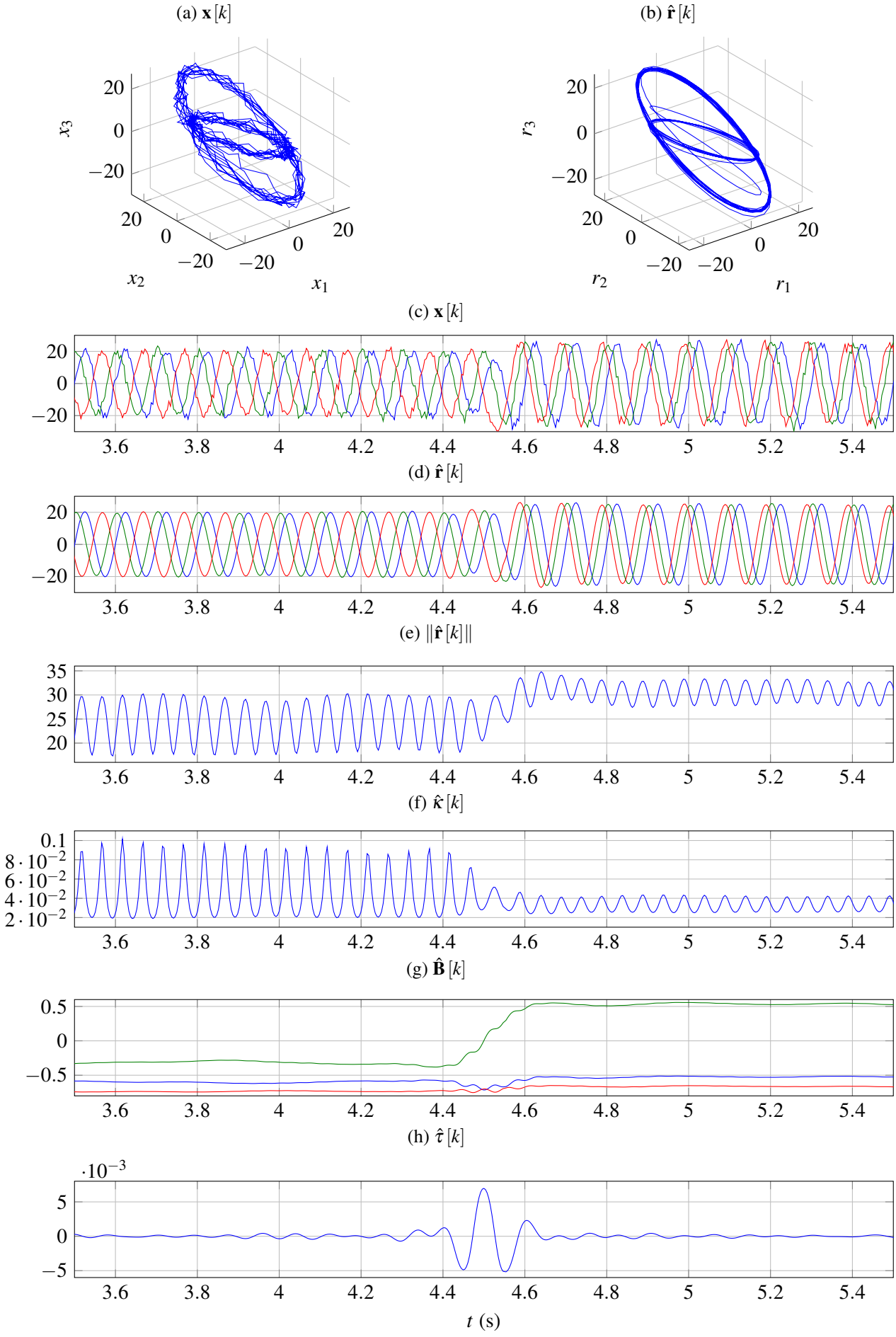

Figure 9: Geometric properties estimation of a three-component simulated signal

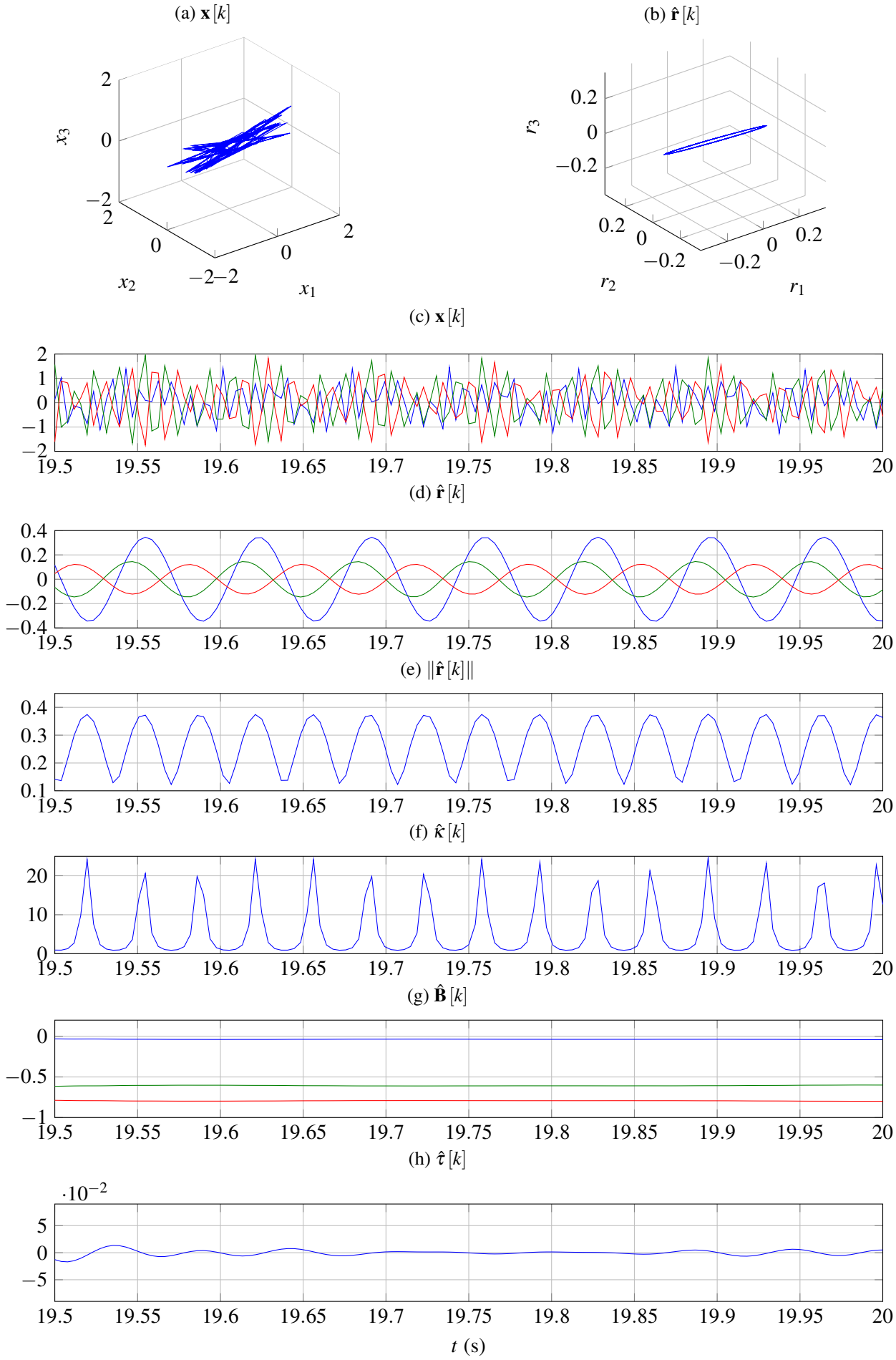

Figure 10: Geometric properties estimation of a three-component experimental signal (electric motor vibrations)

6 Conclusion

A method of estimating the geometric properties of the elliptical trajectory followed by a three-component sinusoidal signal in three-dimensional Euclidean space is proposed in this paper. A simple estimation algorithm is presented and its estimation performance is analyzed. From this analysis, it can be seen that the performance is limited when it comes to low frequency signals with additive noise and in the case of a linear trajectory. The method is validated by applying it to an illustrative synthetic example and a simple experimental signal. Several improvements can be envisaged. The noise removal step can be developped further and other global geometric properties such as the semimajor and semiminor axes a and b of the ellipse as well as its orientation in space can be estimated in a better fashion. Other possible developments include changing domains where instead of representing the signals in the time domain, they are represented in the frequency domain, which can fix filter problems as well as make the method usable for random signals.

References

[1] D. R. Brillinger, *Time Series: Data Analysis and Theory*, Society for Industrial and Applied Mathematics (SIAM), 2001.

[2] P. Granjon, *Complex-Valued Signal Processing for Condition Monitoring*, International Conference on Condition Monitoring and Machinery Failure Prevention Technologies, Edinburgh, Scotland (2008).

[3] P. J. Schreier, L. L. Scharf, *Statistical Signal Processing of Complex-Valued Data*, Cambridge University Press, UK (2010).

[4] N. Bachschmid, P. Pennacchi, A. Vania, *Diagnostic significance of orbit shape analysis and its application to improve machine faults detection*, Journal of the Brazilian Society of Mechanical Sciences and Engineering, Vol. 26, No. 2, 2004, pp. 200-208.

[5] C. C. Lee, Y. S. Han, *The directional Wigner distribution and its applications*, Journal of Sound and Vibration, Vol. 216, No. 4, October 1998, pp. 585-600.

[6] Y. S. Han, C. W. Lee, *Directional Wigner distribution for order analysis in rotating/reciprocating machine*, Mechanical Systems and Signal Processing, Vol. 13, No. 5, September 1999, pp. 723-737.

[7] V. Ignatova, P. Granjon, S. Bacha, *Space vector method for voltage dips and swells analysis*, IEEE Transactions on Power Delivery, Vol. 24, No. 4, October 2009, pp. 2054-2061.

[8] M. P. do Carmo, *Differential Geometry of Curves and Surfaces*, Prentice-Hall, New Jersey (1976).

[9] M. Spivak, *A Comprehensive Introduction to Differential Geometry Volume Two (Second Edition)*, Publish or Perish, Berkeley (1979).

[10] A. J. Hanson, H. Ma, *Visualizing Flow with Quaternion Frames*, IEEE Visualization, Arlington, VA, 1994 Oct 19-21, pp. 156-163.

[11] E. Kreyszig, *Differential Geometry*, Dover Publications, New York (1991).

[12] D. J. Struik, *Lectures on Classical Differential Geometry*, Addison-Wesley, Reading, Mass. (1961).

[13] M. Mandal, A. Asif, *Continuous and Discrete Time Signals and Systems*, Cambridge University Press, UK (2007).

[14] J. G. Proakis, D. G. Manolakis, *Digital Signal Processing: Principles, Algorithms, and Applications (Fourth Edition)*, Pearson Education, NJ (2007).

[15] C. C. Tseng, S. L. Lee, *Linear phase FIR differentiator design based on maximum signal-to-noise ratio criterion*, Signal Processing, Vol. 86, No. 2, February 2006, pp. 388-398.

[16] G. Phua, P. Granjon, *Analysis of three-dimensional physical quantities for system diagnosis*, International Conference on Condition Monitoring and Machinery Failure Prevention Technologies, London (2012).